Paddy Rice Experiment in the Sanjiang Plain (PRESP 2012)

Field Measurement Report

Version 1.0

Hongliang Fang, Wenjuan Li, Shanshan Wei, Tao Sun, Chongya Jiang

State Key Laboratory of Resources and Environmental Information System,
Institute of Geographic Sciences and Natural Resources Research,
Chinese Academy of Sciences

January 2014

Participants

Prof. Hongliang Fang
Principle Investigator
LREIS, Institute of Geographic Sciences and Natural Resources Research
Chinese Academy of Sciences
Beijing 100101, China
Email: fanghl@lreis.ac.cn

Wenjuan Li, Shanshan Wei, Tao Sun, Chongya Jiang
PhD. students
LREIS, Institute of Geographic Sciences and Natural Resources Research
Chinese Academy of Sciences
Beijing 100101, China

Acknowledgments

The field campaign was supported by the National Natural Science Foundation of China (41171333) and the Hundred Talent Program of the Chinese Academy of Sciences. We would like to thank the interns who attended the field work at various stages, and the farmers for allowing us to make use of their fields for in situ measurements.

Revision History

Revision Date	*Changes*	*Major contributor*
2014-1-20	Initial draft	Wenjuan Li

Table of Contents

List of Figures

List of Tables

List of Acronyms and Abbreviations

ACFs	Apparent clumping factors
ALA	Average leaf angle
CI	Clumping index
DHP	Digital hemispheric photography
DOY	Day of year
ESU	Elementary sampling unit
fCover	Fraction of vegetation cover
LAI	Leaf area index
LAD	Leaf angle distribution
LAI-2200 4R	LAI-2200 with the inner four rings
LAI-2200 5R	LAI-2200 with all five rings
LUT	Look up table
PAI	Plant area index
PAI_{eff}	Effective plant area index
PAR	Photosynthetically active radiation
SAI	Stem and seeds area index
SZA	Solar zenith angle
VALERI	Validation of Land European Remote Sensing Instruments
VZA	View zenith angle
YAI	Yellow area index

1. Overview

The Paddy Rice Experiment in the Sanjiang Plain (PRESP) was conducted at the paddy rice fields in Honghe Farm, NE China (47°39.11′ N，133°31.31′ E), from mid-June to mid-September 2012. The objective of the field campaign is to collect consistent ground LAI data for paddy rice in order to support the validation of LAI products obtained by remotely sensed data. The site is about 3 km × 3 km with five plots scattered in four corners and the center. Several optical instruments, including LAI-2200, Digital Hemispheric Photography (DHP), and AccuPAR and the destructive methods were used to obtain LAI and other structural parameters (Table 1).

Table 1. Structural variables derived from field measurement methods.

	LAI-2200	DHPs	AccuPAR	Destructive
PAI		√		√
PAI_{eff}	√	√	√	
LAI				√
YAI				√
SAI				√
Angular Gap fraction	√	√		
Integrated gap fraction or transmittance	√	√	√	
CI	√	√		
ACF	√			
ALA	√	√		
fCover	√	√		

2. Site description and ground sampling

2.1 Site description

The study area is located at the Honghe Farm in the Heilongjiang Province, NE China (Fig. 1). The site experiences a typical humid continental monsoon climate, with long cold winter and warm and humid summer. The mean annual temperature is 2.52 °, with monthly mean temperature ranging from -20 ° in January to about 22 ° in July. The average annual precipitation is approximately 558 mm, with substantial interannual and seasonal variation (Song et al., 2009). The mean altitude of this site is approximately 56 m. The main soil types are the albic bleached meadow soils (Albaqualfs) (Yang et al., 2013). The water and soil in these marshes are completely frozen from late October to April and begin to thaw in late April.

This site was originally a wetland and has been converted to plant paddy rice since 1997. The paddy rice fields are flat with more than 5 km homogeneity and large rectangular fields approximately 30 m × 100 m in size. A single rice variety (Japonica) is grown in this region. The rice-cropping practices are uniform, growing once a year during the summer season (May to September), with a maturation stage for about 120-150 days. The dates for the panicle formation stage, heading stage, and maturity stage are mid-June, mid-July, and early August, respectively. Paddy fields are irrigated with ground water throughout the season. The soil surface is under flooded conditions during most of the growing periods.

2.2 Sampling strategy

Five plots (A, B, C, D, and E), four at the four corners and one at the center, were chosen for intensive ground based measurements (Fig. 1). Each plot was planted with a cultivar type and managed individually. Small differences exist among the plots in terms of the plant density and plantation methods (Table 2). Within each plot, 50 ~ 60 Elementary Sampling Units (ESUs), in the size of 15×15 m^2 or 20×20 m^2 were selected. ESUs were located at least 1.5 m away from the field borders. The main information of five plots is showed in Table 2.

In order to reduce the impact of destructive sampling and measurement disturbance, a moving sampling strategy was adopted. Four ESUs within a plot were selected in the first week and LAI measurements were taken for each ESU using one method. Used ESUs will be discarded and another four parallel ESUs will be selected for the next week. ESU-level sampling was performed along a diamond box with two 15-meter diagonals as recommended by the VALERI network (Validation of Land European Remote Sensing Instruments, http://w3.avignon.inra.fr/valeri/).

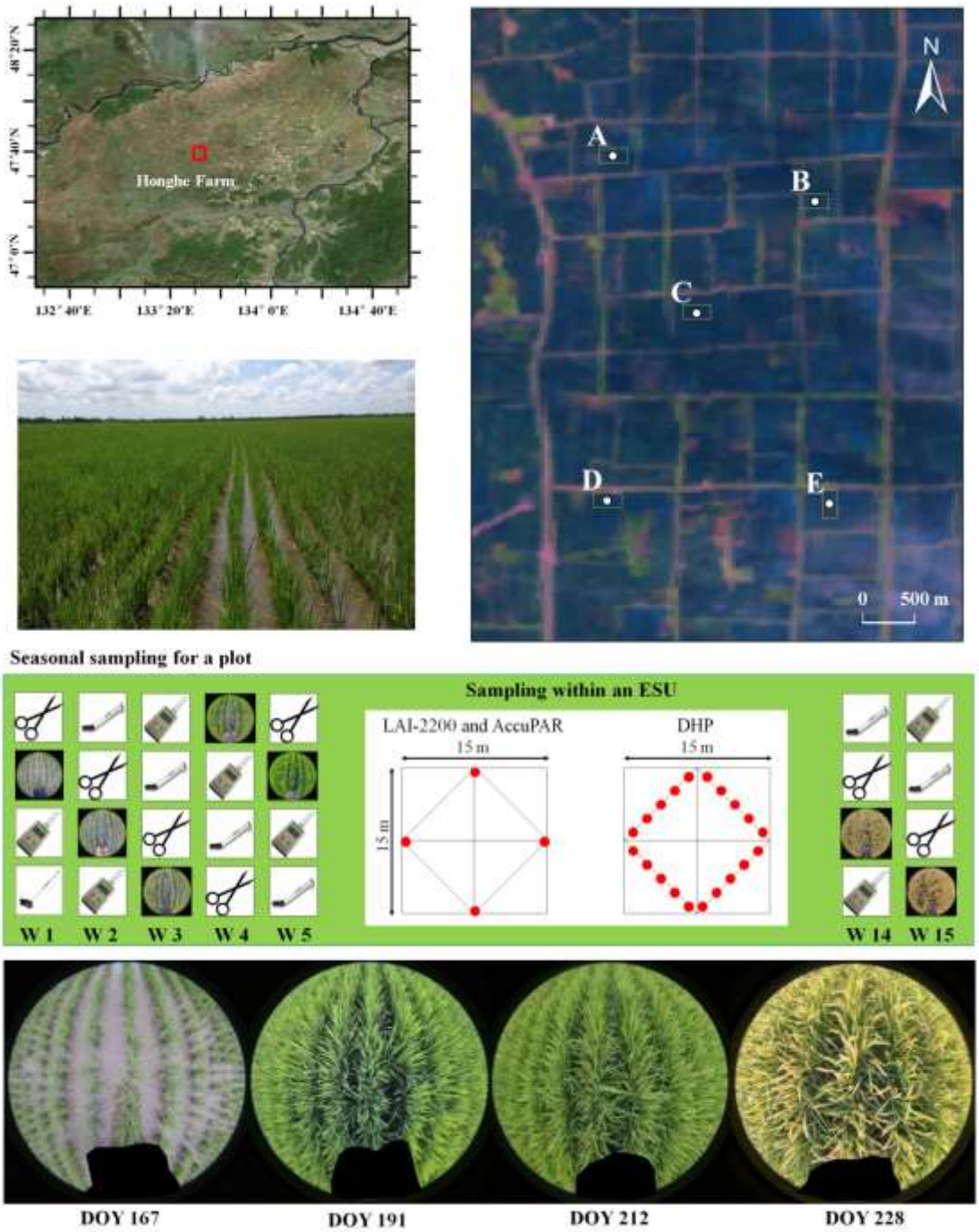

Fig. 1 The upper panel shows the location of the site on Bing™ images, a photo taken in a paddy rice field and the distribution of five plots on a Landsat-7 ETM+ image (June 3, 2012). The middle panel shows the seasonal sampling strategy for a plot and within an ESU for LAI-2200, AccuPAR and DHP ('W' represents week). The bottom panel shows the downward DHP images obtained during different stages of leaf development.

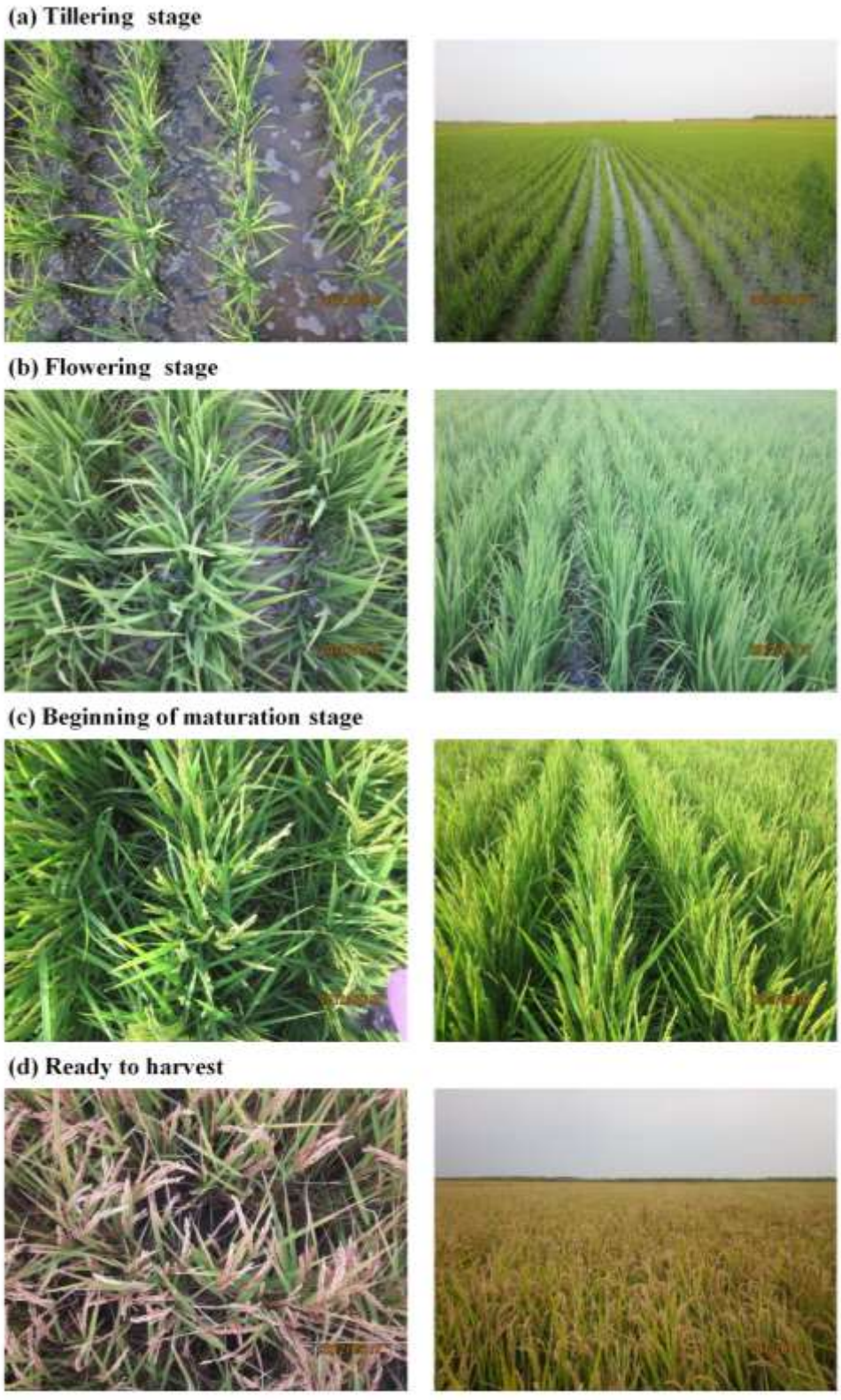

Fig. 2. Sample photos for the main growing stages: (a) tillering stage (Jun 18, 2012); (b) flowering stage (Jul 13, 2012); (c) beginning of maturation stage (Aug 2, 2012); (d) ready for harvest (Sep 12, 2012).

Table 2. Information for the five plots in the study area.

Plot ID	Center location	Density (plants/m^2)	Inter-row distance (m)	ESU size (m)
A	133.515 °E, 47.667 °N	25	0.288	10×10
B	133.532 °E, 47.663 °N	26	0.286	10×10
C	133.523 °E, 47.653 °N	24	0.299	15×15
D	133.515 °E, 47.637 °N	28	0.283	15×15
E	133.534 °E, 47.637 °N	28	0.274	15×15

Ground LAI measurement was conducted from June 11, shortly after the rice transplantation, to September 17 when the rice was ready for harvest. Fig. 2 shows some photos taken at the main growing stages in the study area. Field measurements were performed sequentially for the five plots every week, in order to capture the canopy structural dynamics. All optical measurements were conducted near sunset or under overcast conditions as the sensitivity of the parameters and the retrieval errors increase under direct illuminations (Garrigues et al., 2008). Major morphological changes, rice height, water depth and field conditions during this period were also observed and recorded (Table 4). The radiation, PAR, temperature, and relative humidity were obtained at a nearby weather station managed by the Sanjiang Marsh and Wetland Ecological Experiment Station, Chinese Academy of Sciences (Fig. 3).

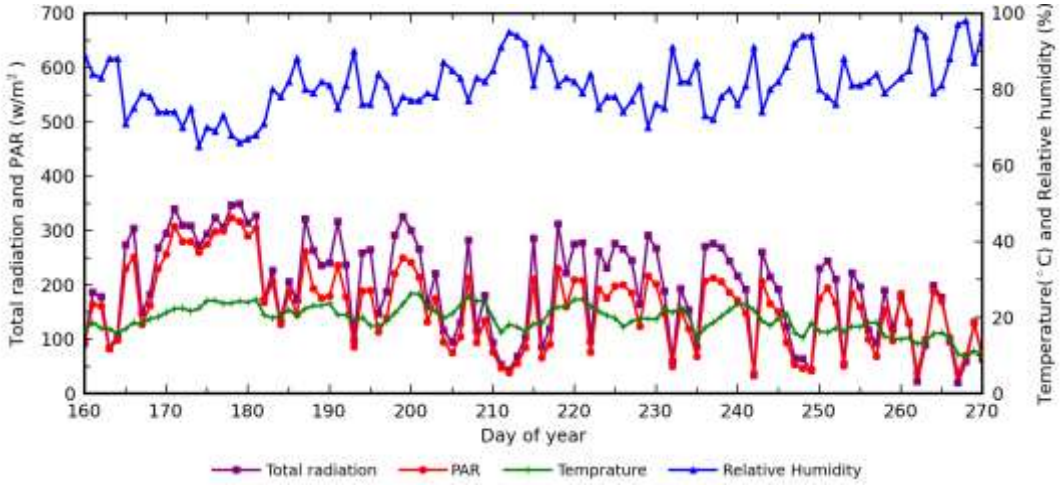

Fig. 3. Radiation, PAR, temperature, and relative humidity for the site in 2012.

3. Field measurement methods

3.1 LAI-2200

A LAI-2200 Plant Canopy Analyzer (PCA) (LI-COR Inc., Lincoln, Nebraska) was used to estimate the rice PAI as all parts of the plants, including green leaves, yellow leaves, stems, and seeds contribute to the canopy transmittance process (Fig. 4). All measurements were conducted under diffuse conditions. Following the instruction manual for row crops, ground measurements were made along diagonal transects between the rows (Fig. 5). Two repeats were made for each measurement with one above and four below canopy readings (Fig. 6). For below canopy measurements, the instrument was held about 5 cm above the background soil or shallow water. Throughout the season, a 270° view cap was used to shield the sensor from the operator. All values from four measurements were averaged to obtain the values at the ESU level.

Fig. 4. LAI-2200 with a single sensor

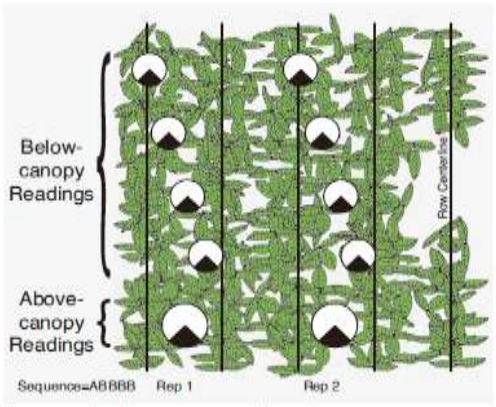

Fig. 5. Sampling strategy for LAI-2200 over paddy rice field

Fig. 6. LAI-2200 field measurement method (left: above the canopy; right: below the canopy)

Five concentric conical rings, 7 °, 23 °, 38 °, 53 °, 67 °, were used to record the incident light under and above the canopy.

The average probability of light penetration into the canopy is computed by

$$\overline{P(\theta_i)} = \frac{1}{N_{obs}} \sum_{j=1}^{N_{obs}} \frac{B_{ij}}{A_{ij}} \quad (1)$$

where the subscript i (i = 1 … 5) refers to the optical sensor rings centered at θ_i and j refers to the number of observational pairs (j = 1 … N_{obs}). B_{ij} and A_{ij} are the j^{th} below and above canopy readings, respectively, for the i^{th} ring. The gap fraction for the i^{th} ring is computed from

$$G_i = e^{(\overline{\ln P(\theta_i)})} = e^{(\frac{1}{N_{obs}} \sum_{j=1}^{N_{obs}} \ln \frac{B_{ij}}{A_{ij}})} \quad (2)$$

Assuming the foliage elements are randomly distributed in space, the effective PAI (PAI_{eff}) can be estimated by the transmittance in the different view angles based on Miller's formula (Miller, 1967).

$$PAI_{eff} = 2\int_0^{\pi/2} -\ln P(\theta) \cos\theta \sin\theta d\theta \quad (3)$$

Since multiple observations of $P(\theta)$ are available for LAI-2200, the effective PAI is calculated as

$$PAI_{eff} = 2\int_0^{\pi/2} -\overline{\ln P(\theta)} \cos\theta \sin\theta d\theta = 2\sum_{i=1}^{5} \overline{K_i} W_i \quad (4)$$

where K_i and W_i are the contact number and the weighting factor, respectively (Table 3).

The typical PAI_{eff} provided by LAI-2200 is calculated on five rings. For comparison purpose, four-ring PAI_{eff} was also calculated from the four inner rings using FV-2200™ accompanied with LAI-2200 by excluding the fifth ring from the calculation.

Table 3. The weighting factors of each ring for LAI-2200 and LAI-2000.

Ring number	Ring center	Weighting factors	
		LAI-2200	LAI-2000
1	7	0.041	0.034
2	23	0.131	0.104
3	38	0.201	0.160
4	53	0.290	0.218
5	68	0.337	0.494

Compared to the LAI-2000, LAI-2200 has changed the weighting factors for the five rings (Table 3). Moreover, LAI-2200 provides the Apparent Clumping Factor (*ACFs*) using the gap fraction measured by five rings (Ryu et al., 2010). *ACFs* has been considered representing the maximum clumping index for canopy.

$$ACF_s = \frac{2\int_0^{\pi/2} -\frac{\ln \overline{P(\theta)}}{S(\theta)} \sin\theta d\theta}{2\int_0^{\pi/2} -\frac{\overline{\ln P(\theta)}}{S(\theta)} \sin\theta d\theta} = \frac{2\sum_{i=1}^{5} -\frac{\ln \overline{P(\theta_i)}}{S_i} W_i}{2\sum_{i=1}^{5} \overline{K_i} W_i} \quad (5)$$

LAI-2200 calculates the foliage mean tilt angle based on Lang (1986), using an empirical polynomial relating inclination angle to the slopes of the idealized curves between 25 ° and 65 °.

The fractional vegetation cover (*fCover*) is calculated by:

$$fCover = 1 - P(7^\circ) \quad (6)$$

where $P(7^\circ)$ is the gap fraction measured on the first ring center at 7 °.

3.2 DHP

The DHP images were taken using a Nikon D5100 camera and a 4.5 mm F2.8 EX DC circular fisheye convertor (Fig. 7). An ultraviolet cap was used to prevent dust or rain from the lens. The total height of camera and the lens was about 16.5 cm. Two bubble levels were attached to the camera to keep it horizontal for both downward and upward viewing directions. System calibration for DHP camera was performed before measurement according to the CAN_EYE manual (version 6.3.3), in order to get the optical center and projection function of the lens (Weiss and Baret, 2010).

Fig. 7. Nikon D5100 equipped with Sigma F2.8 EX DC circular fisheye. An ultraviolet cap was used to prevent dust or rain from the lens.

Downward-looking photos were taken before July 10 (DOY 192) when the rice began to enter the flowering stage (Fig. 8a). The distance between the camera and the top canopy was set to about 0.8-1.5 m to avoid individual leaves too close to the camera. When the rice grew higher than 70 cm (after July 10), upward-looking photos were also taken at the same location of the downward measurements (Fig. 8b and 8c). For the upward measurements, the camera was placed right above the ground soil or water. Before July 26 (DOY 208), the camera was set to automatic exposure to prevent the saturation issues during the downward measurement (Demarez et al., 2008). After that, the aperture and shutter speed of the camera were manually adjusted to avoid over-exposure because the sunlight intensity may change greatly during the measurement direction shifts. To properly sample the spatial variability of the ESU, at least 20 hemispherical photos with single direction were taken along the diamond strategy (Fig. 1). Nearly all photos were taken under overcast illumination to minimize the shadow effect. All images within an ESU were considered to be under similar illumination conditions. These photos were stored in high-quality JPEG format at a resolution of 3264×4928.

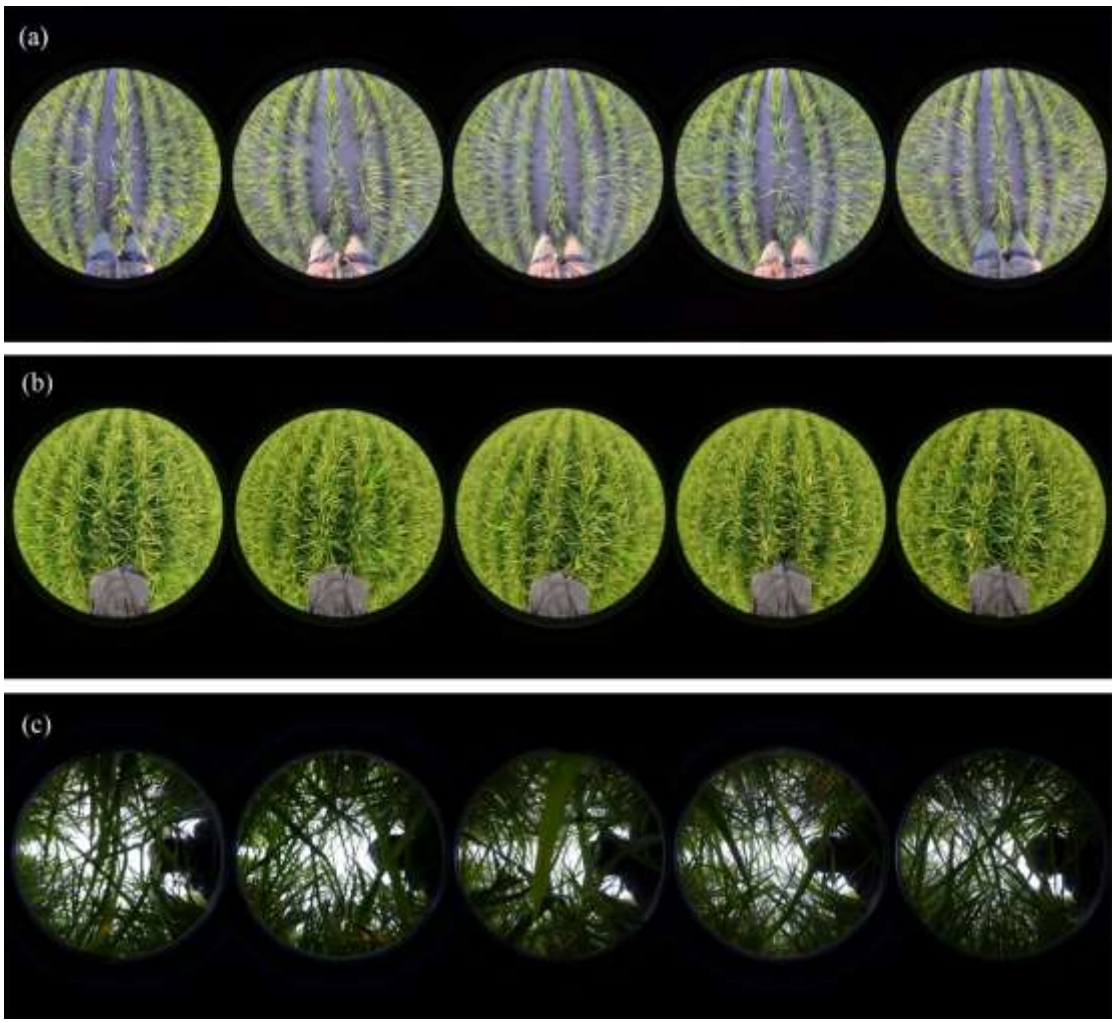

Fig. 8. (a) Downward-looking photos for low rice canopy (< 0.7 m, before Jul 7). When rice grew higher (> 0.7 m, enter flowering stage), both downward photos (b) and upward photos (c) were taken.

All valid photos (8~20) over one ESU were processed simultaneously by the CAN_EYE software (version 6.3.3) to extract the structural variables (Weiss et al., 2004). The limit of image in viewing degrees used in this research (COI) was set to 60 ° by default. To get a balance between the computation time and images amount, angular resolution for zenith and azimuth directions were set to 10 ° and the solid angle used in computing the cover fraction was also set to 10 °. A threshold process is necessary to separate the foliage from the soil background (downward view) or the sky (upward view). To minimize subjective errors, one operator performed all thresholding and classification processes. Fig. 9 presents an example for the downward DHPs classification results in CAN_EYE. More detailed processing procedures can be found in the CAN_EYE manual (version 6.3.3).

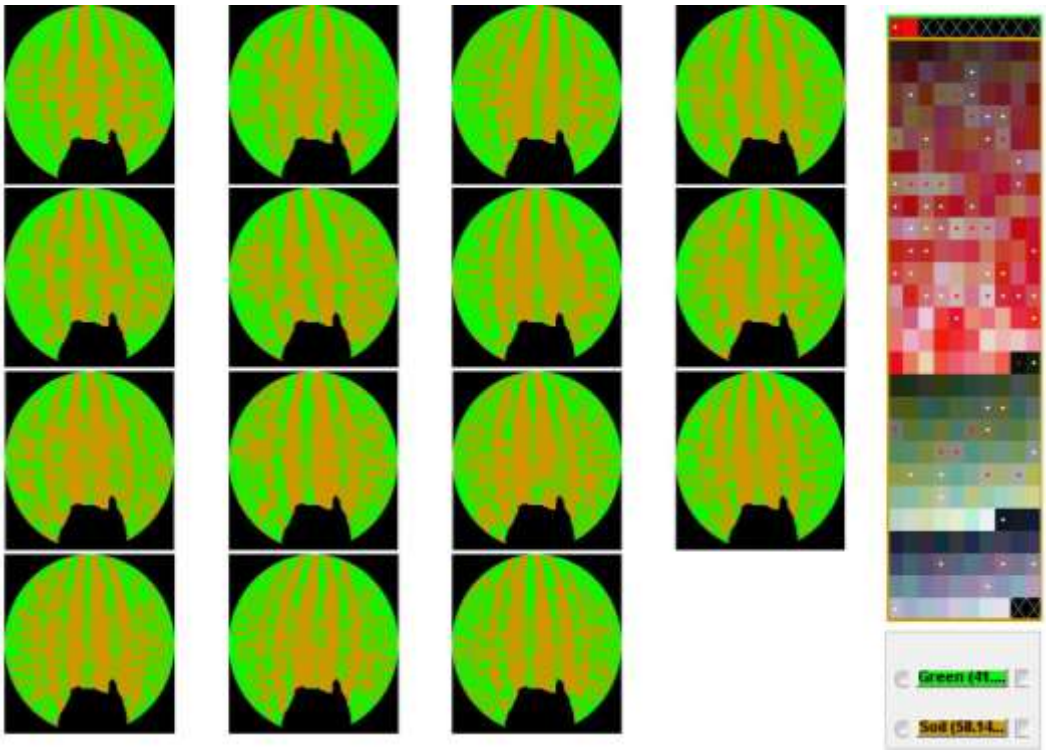

Fig. 9. An example of photo classification in the CAN_EYE software. Green indicates the rice and soil is the background. The operators have been masked.

Assuming an ellipsoidal distribution of the leaf inclination, PAI_{eff} is retrieved using look-up-table techniques with CAN_EYE (Weiss and Baret, 2010). A large range of random combinations of LAI (0 ~ 10) and ALA (10 °~ 80 °) values are used to build a database following the Beer-Lambert's law (Nilson, 1971):

$$P(\theta) = e^{-G(\theta)\cdot PAI_{eff} / \cos(\theta)} \quad (7)$$

where $P(\theta)$ is the canopy gap fraction at direction θ and $G(\theta)$ is the projection function. By comparing the measured gap fraction and those stored in look-up-table, effective PAI and ALA can be retrieved from Eq. (7) by setting a cost function.

The regularization cost functions used in CAN-EYE V5.1 (Eq. 7 in Weiss 2010) and V6.1 (Eq. 8 in Weiss 2010) are different. V5.1 tries to constrain the retrieved ALA to be within $60° \pm 30°$, whereas V 6.1 tries to minimize the difference between the retrieved PAI and that estimated from the $57°$ observations. The constraints on V6.1 are efficient without any assumption on ALA; therefore, the V6.1 results are mainly considered for further analysis in this report.

The clumping index (CI) at direction θ is computed using the logarithm gap fraction averaging method (Lang and Xiang, 1986):

$$CI(\theta) = \frac{\ln \overline{P(\theta)}}{\overline{\ln P(\theta)}} \tag{8}$$

The fraction of vegetation cover (*fCover*) is calculated as the fraction of the soil covered by the vegetation viewed in the nadir direction.

$$fCover = 1 - P(\theta_{\min}) \tag{9}$$

where $P(\theta_{\min})$ is the gap fraction measured at the smallest view angle $\theta_{\min}$ (10°).

3.3 AccuPAR

Decagon's AccuPAR model LP-80 PAR/LAI ceptometer measures photosynthetically active radiation (PAR) using 80 individual sensors (zenith angle is 90°) on its probe (Fig. 10). It measures PAR by locating the probe under and above the canopy and then computes PAI based on angularly integrated transmittance (Fig. 11). Before each measurement, AccuPAR was calibrated according to the instruction manual (when the above canopy PAR is larger than 600 umol/m^2s). In the field, AccuPAR measurements were taken before all the other optical measurements due to the sensitivity of the PAR sensor to the radiation intensity.

Fig. 10. AccuPAR model LP-80 PAR/LAI ceptometer

Fig. 11. Below canopy PAR measurements in four directions with AccuPAR.

For AccuPAR, the effective PAI is derived following the equations to predict the scattered and transmitted PAR (Norman and Welles, 1983).

$$PAI_{eff} = \frac{[(1-\frac{1}{2k})f_b - 1]\ln\tau}{A(1-0.47f_b)} \quad (10)$$

where τ is the transmission coefficient obtained through the ratio of the below canopy and the above canopy PARs, f_b is the fraction of incident beam PAR, A is a function of the leaf absorptivity *(a)* in the PAR band (AccuPAR assumes a = 0.9, and A=0.86 in LAI sampling routines), and k is the extinction coefficient for the canopy (default value: 1.0).

3.4 Destructive method

In the field, five bundles were randomly harvested at water level in each ESU, placed in a sealed plastic bag and stored inside a cooler box (Fig. 12). The distance between rows and plants, the plant height and water depth were randomly measured five times. The average value of five measurements was used to represent the ESU (Table 4). The plant density of the ESU was estimated by calculating the number of plants within a square meter. The average value of all ESU was the plant density of a plot (Table 2).

Ex situ measurements were taken immediately after returning lab. Green leaves were separated from yellow leaves, stems and head components. If a larger proportion of leaves was green (yellow), they were recognized as green (yellow) leaves. The areas of leaves, young stems and seeds were measured with a leaf area meter (model LI-3100C, LI-COR: Lincoln Inc., Nebraska, U.S.) (Fig. 13). After June 19 (DOY 171), the rice stems were too thick for the area meter. In this case, the stems were scanned by a laser scanner (Fig. 14). Seeds were also scanned by the scanner to compare with the LI-3100C results. The rice tissues were put on a white paper and scanned using a CanoScan LiDE 110 laser scanner at a 300 dpi resolution. The scanned images were processed by a thresholding code to separate the rice tissues from the white background.

Fig. 12. Cut rice above the water (left) and preserve them in a cooler box (right).

Fig. 13. Scan leaves and young stems by LI-3100C.

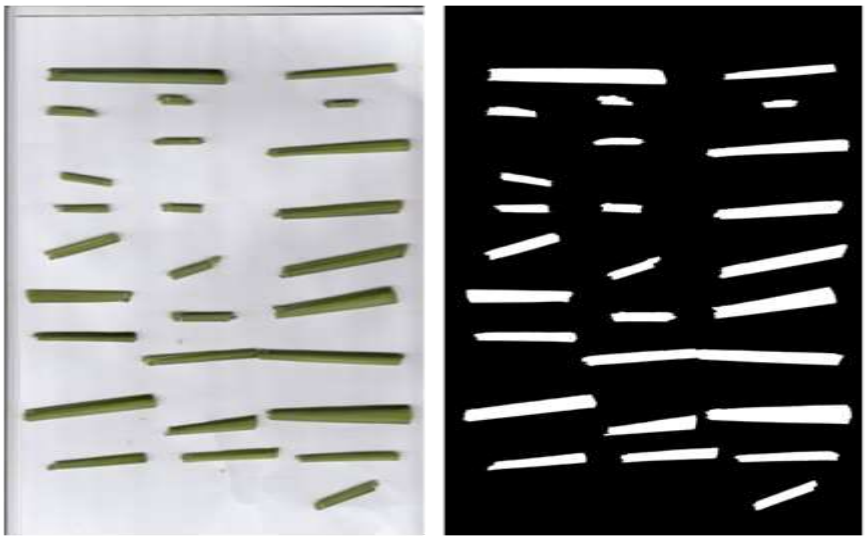

Fig. 14. Scanned stems in a scanner (left) and binaries them to collect pixels area (right).

Based on all above measurements, green area index (LAI), yellow area index (YAI), stem and seeds area index (SAI), and plant area index (PAI) were calculated as the result of the average area index by the ESU 's plant density.

$$Density = \frac{1}{d_r \cdot d_p} \tag{11}$$

$$PAI = LAI + YAI + SAI \tag{12}$$

where d_r is the row distance and d_p is plant distance for each plot.

4. Results

For each plot, data over the season were interpolated to obtain a consecutive profile from DOY 163 to DOY 261. Then the site-level value was calculated by averaging data over five plots.

4.1 Destructive PAI

For all non-flat elements (stems, ears, and rolled leaves), the projected area was estimated in a way similar to the indirect optical observations (Fig. 2 in (Fang et al., 2014)). Other studies have considered the developed surface area (Baret et al., 2010; Lang et al., 1991; Stenberg, 2006). However, it is rather difficult to extend and measure the flat surface area of the rolled senescent leaves. If stems are treated as cylinders, the ratio of half the total surface area of the convex hull to the projected area is $\pi/2$, i.e., 1.57 (Fig. 15).

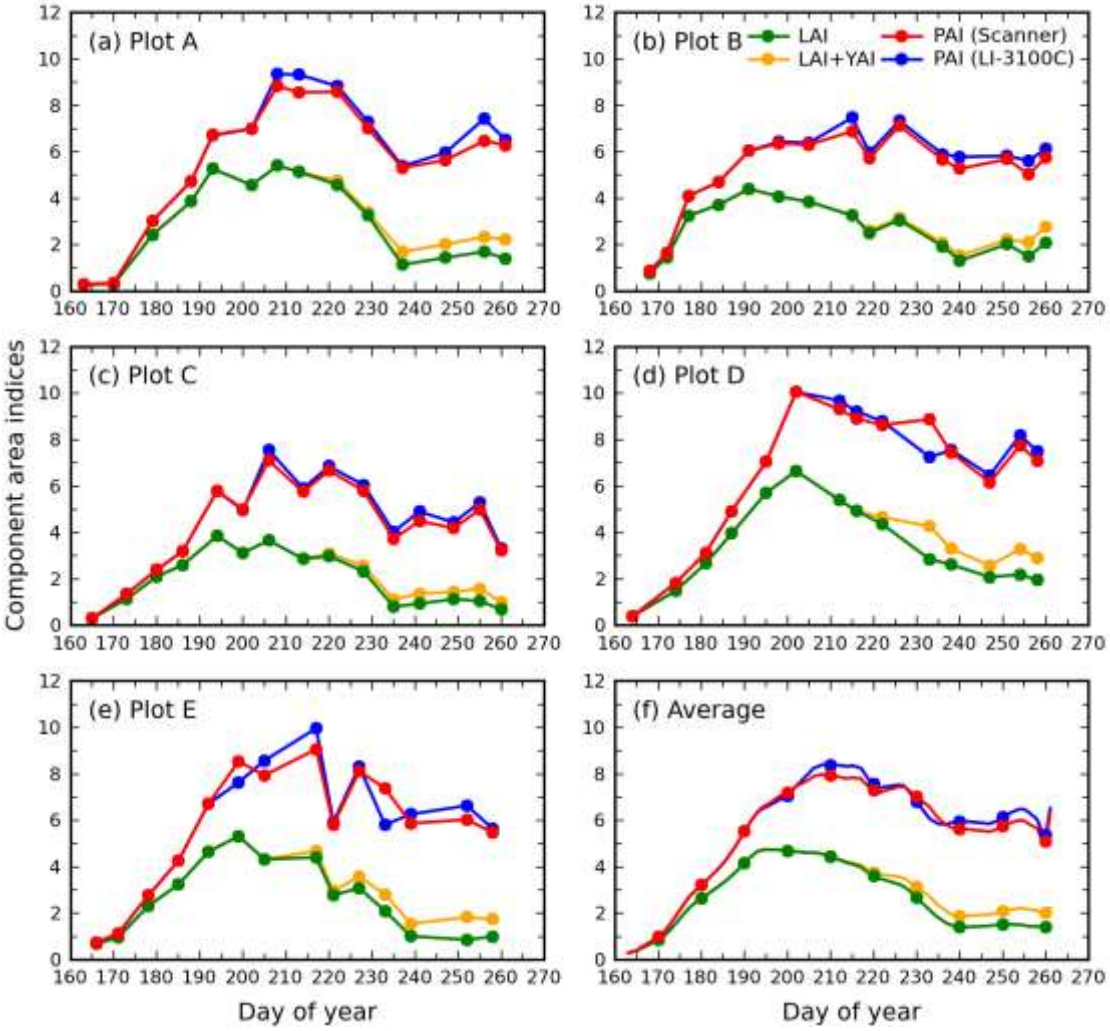

Fig. 15. Seasonal variation of LAI and PAI values calculated as the developed surface area. The average data for five plots are presented in (f).

4.2 Effective PAI

The effective PAI estimated from LAI-2200, the downward and upward DHPs, and AccuPAR have been shown in Fang et al. (2014).

4.3 Gap fraction

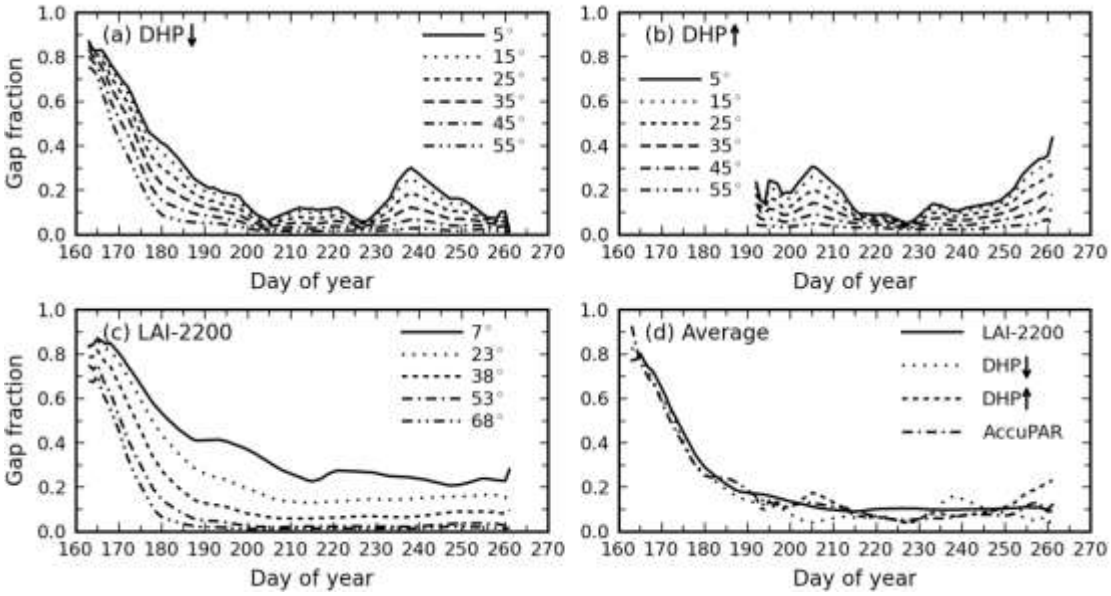

Fig. 16. Seasonal variation of the average gap fraction at different view zenith angles from LAI-2200 and downward and upward DHPs. For DHPs, the modeled effective gap fractions from CAN_EYE V6.1 are shown. Panel (d) shows the average gap fractions from LAI-2200 and DHPs and the transmittance from AccuPAR.

The modeled gap fractions for DHPs retrieved from CAN_EYE V6.1 are shown in Fig. 16. On average, the gap fraction for the downward DHP is slightly lower than that of the LAI-2200 (-0.028), except for DOY 240. The gap fraction for the upward DHP is similar to that of the LAI-2200 before DOY 250 (average difference:-0.002), and higher (0.06) than LAI-2200 after the date. The modeled gap fraction from the downward DHP is systematically lower than that of the AccuPAR (-0.01), while the upward DHP value is higher than the AccuPAR (0.02). The measured gap fractions for the downward and upward DHPs have been shown in Fang et al. (2014).

4.4 Clumping index

Fig. 17 presents the seasonal dynamics of CI estimated from the downward and upward DHPs and the ACF from LAI-2200. CI generally decreases with the increase of view zenith angle for the upward DHP in the whole season and for the downward DHPs after DOY 171. On average, the downward CI is larger than the upward CI by about 0.085 after DOY 191. In contrast, ACF from LAI-2200 shows little seasonal

variation for all angles. The average ACF is systematically higher than the CI values estimated from the downward and upward DHPs, by 0.23 and 0.34, respectively.

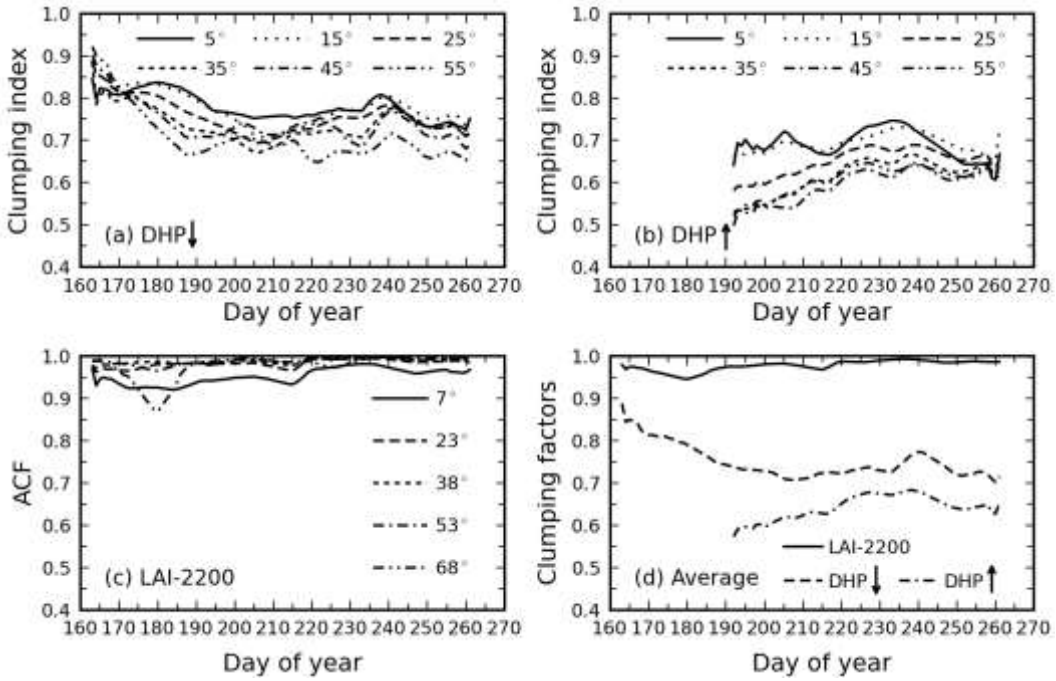

Fig. 17. Seasonal variation of the average clumping indices from, (a) the downward DHP, (b) the upward DHP and (c) LAI-2200. Panel (d) shows the angular average of CI values.

4.5 ALA and fCover

4.5.1 Seasonal trend of ALA calculated from LAI-2200 and DHPs

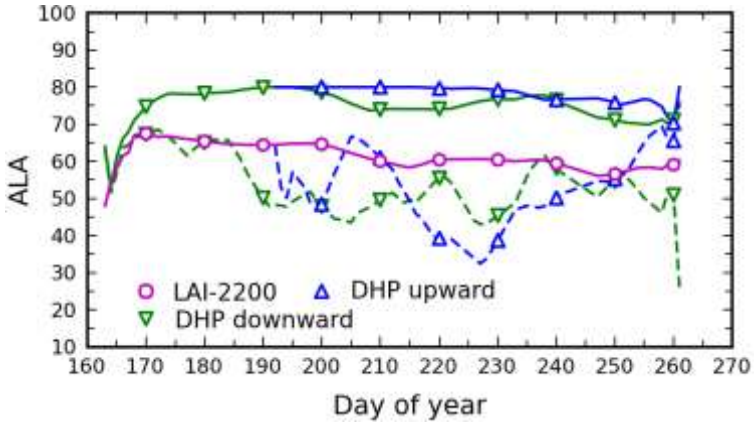

Fig. 18. Seasonal variation of ALA calculated from LAI-2200, downward DHP and upward DHP. Solid and dashes lines represent true and effective ALAs retrieved from DHPs, respectively.

The seasonal dynamics of ALAs estimated from LAI-2200, downward and upward DHPs are presented in Fig. 18. ALA from LAI-2200 shows little seasonal variation, with a mean value of 64.3 ° from DOY 160 to 200, and 59.67 ° after DOY 200. In contrast, the effective ALA from the DHPs shows strong variations ranging from 26.1 ° to 75.4 °. The average effective ALA from downward and upward DHPs are 53.74 ° and 52.31 °, respectively. The true ALA retrieved from the downward and upward DHPs show little seasonal variations, with average ALAs values at about 75.05 ° and 78.41 °, respectively. The true ALAs are systematically higher than the effective ALAs, by about 13.67 °~ 26.1 °.

4.5.2 Seasonal trend of fCover calculated from LAI-2200 and DHPs

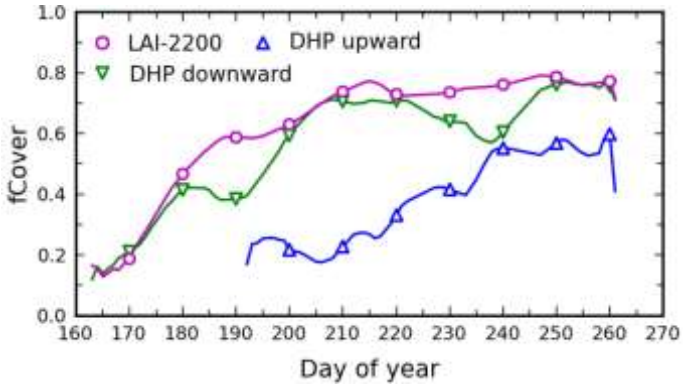

Fig. 19. Seasonal variation of fCover calculated from LAI-2200, downward DHP and upward DHP.

The seasonal variation of fCover estimated from LAI-2200, downward and upward DHPs is shown in Fig. 19. The fCover estimated from all optical instruments increases with the season. The mean fCover values from LAI-2200, downward DHP and upward DHP are 0.62, 0.56 and 0.39, respectively. The fCover estimated from the upward DHP is systematically lower than those from the downward DHP and LAI-2200, by 0.17 and 0.24, respectively. Note that the fCover is calculated from the gap fraction, and it represents the whole coverage including green leaves, yellow leaves, stems and seeds.

5. Quality assurance

The study area is considered homogeneous at a 3 × 3 km^2 area. The five plots are located away from the road, irrigation canals and ditches. The field management practices and environmental conditions are similar for these plots. Weekly field measurement began right after the transplantation and ended when the rice was ready for harvest. Nearly all measurements were performed under diffuse radiation condition, i.e., near the sunset or during overcast days.

The optical instruments were newly purchased and were tested before the field campaign. Instrument calibrations were performed before or during the measurements, according to the instrument manual. However, unexpected incidents have happened during the field work and they are noted in Table 4.

For LAI-2200, the direct illumination could happen and the 270° view cap was missing for several occasions. Measurement for Plot B on August 2 was conducted under direct radiation with a 90° view cap and the measurements for Plot D on August 20 was also under the direct illumination condition with a 270° view cap. No view cap was used for Plot B on September 6, for Plot C on August 22, August 28 and September 5, and for Plot E on September 8 because the 270° view cap was missing during the measurements. Furthermore, unreliable data with very small above-canopy radiation readings (< 10°) were also deleted, including the measurements for Plot A (July 31), Plot B (July 16), Plot C (August 22 and September 16), Plot D (July 30) and Plot E (August 20).

The downward DHP photos taken over Plot A on July 11 and July 31, over Plot C on July 18, and over Plot E on August 4 were too dark for classification and were excluded. The upward photos taken for Plot B on August 27 were also deleted due to the dark sky.

When the PAR value is less than 10 umol/m^2s, the AccuPAR measurements were not used. Measurements at Plots A on July 31 and at Plot E on July 10 were purged from further analysis due to the low PAR readings.

For the destructive method, seeds collected for Plot E on July 17 were only measured by the scanner. The LI-3100C was out of work for nearly one week (August 20 – August 27) (Table 4). Accordingly, the bundles collected for Plot D and E on August 20 were all scanned by the scanner, with leaves sticked to white papers by tapes. Moreover, seeds were only scanned by the scanner for Plot E on August 20. The rice bundles for Plot A (August 24), and Plot B (August 27) were frozen in a refrigerator and processed using the LI-3100C after it resumed working.

Table 4. Major morphological changes, rice height, water depth and instruments conditions during the measurement.
From left to right: plot ID, measurement dates, Day of year, phenological stage (TL: tillering, FL: flowering, GF: grain filling, MA: maturation, including yellow maturation), average height of the plants, wetness of the soil, depth of soil water (W: wet, WS: water saturate, WL: water logged), the sky illumination condition (Dif: diffuse dominant, Dir: direct sunlight, Block: the direct sun was obscured by cloud during measurements), green leaves measurements, ears appearance, yellow leaves appearance, LAI-2200 view cap (VC) status (HM: handmade 270 °), AccuPAR status, the number of photos for the downward looking DHPs and upward looking DHPs, and the LI3000C usability status. Symbol '√' represents all data are good and '-' represents no measurements or no good data.

ID	Dates	DOY	Pheno.	H (m)	Soil	WD (m)	Sky	Green leaves	Seed	Yellow leaves	LAI-2200	AccuPAR	DHP(↓)	DHP(↑)	LI3000C
A	2012/6/11	163	TL	0.21	WL	0.05	Dif	√	-	-	√	√	20	-	√
A	2012/6/18	170	TL	0.32	WL	0.10	Dif	√	-	-	√	√	20	-	√
A	2012/6/27	179	TL	0.43	WL	0.06	Dif	√	-	-	√	√	20	-	√
A	2012/7/6	188	FL	0.62	WL	0.08	Dif	√	-	-	√	√	20	-	√
A	2012/7/11	193	FL	0.69	WL	0.10	Dif	√	√	-	√	√	-	15	√
A	2012/7/20	202	FL	0.96	WL	0.06	Dif	√	√	-	√	√	20	19	√
A	2012/7/26	208	FL	0.95	WL	0.06	Dif	√	√	-	√	√	20	20	√
A	2012/7/31	213	FL	0.86	WL	0.10	Dif	√	√	-	-	-	-	9	√
A	2012/8/9	222	GF	0.91	WL	0.02	Dif	√	√	√	√	√	20	15	√
A	2012/8/16	229	GF	0.97	WS	0.00	Dif	√	√	√	√	√	20	18	√
A	2012/8/24	237	GF	0.91	W	0.00	Dif	√	√	√	√	√	20	20	√
A	2012/9/3	247	MA	0.88	W	0.00	Dif	√	√	√	HM VC	√	20	20	√
A	2012/9/12	256	MA	1.00	WL	0.02	Dif	√	√	√	√	√	20	20	√
A	2012/9/17	261	MA	1.00	W	0.00	Dif	√	√	√	√	√	20	20	√
B	2012/6/16	168	TL	0.29	WL	0.09	Dif	√	-	-	√	√	20	-	√
B	2012/6/20	172	TL	0.31	WL	0.10	Dif	√	-	-	√	√	20	-	√
B	2012/6/25	177	TL	0.41	WL	0.06	Dif	√	-	-	√	√	20	-	√
B	2012/7/2	184	TL	0.52	WL	0.03	Dif	√	-	-	√	√	20	-	√
B	2012/7/9	191	FL	0.66	WS	0.00	Dif	√	-	-	√	√	20	-	√
B	2012/7/16	198	FL	0.80	WS	0.00	Dif	√	√	-	-	√	20	15	√
B	2012/7/23	205	FL	0.81	WS	0.00	Dif	√	√	-	√	√	20	10	√
B	2012/8/2	215	GF	0.95	WL	0.08	Dir	√	√	-	90 °VC	√	20	20	√
B	2012/8/6	219	GF	0.86	WS	0.00	Block	√	√	√	√	√	20	16	√

B	2012/8/13	226	GF	0.81	W	0.00	Dif	√	√	√	√	√	20	20	√
B	2012/8/23	236	GF	0.85	W	0.00	Dif	√	√	√	√	√	20	20	√
B	2012/8/27	240	GF	0.82	W	0.00	Dif	√	√	√	270 °+NO	√	12	-	√
B	2012/9/6	250	MA	0.83	WL	0.01	Dif	√	√	√	No VC	√	14	20	√
B	2012/9/12	256	MA	0.91	WL	0.01	Dif	√	√	√	√	√	20	20	√
B	2012/9/16	260	MA	0.90	W	0.00	Dif	√	√	√	√	√	20	20	√
C	2012/6/13	165	TL	0.21	WL	0.14	Dif	√	-	-	180 °VC	√	20	-	√
C	2012/6/21	173	TL	0.37	WL	0.13	Dif	√	-	-	√	√	20	-	√
C	2012/6/28	180	TL	0.46	WL	0.11	Dif	√	-	-	√	√	20	-	√
C	2012/7/4	186	TL	0.53	WL	0.09	Dif	√	-	-	√	√	20	-	√
C	2012/7/12	194	FL	0.78	WL	0.12	Dif	√	√	-	√	√	20	-	√
C	2012/7/18	200	FL	0.84	WL	0.09	Dif	√	√	-	√	√	-	9	√
C	2012/7/24	206	FL	0.90	WL	0.04	Dif	√	√	-	√	√	8	20	√
C	2012/8/1	214	GF	0.95	WL	0.08	Dif	√	√	-	√	√	20	15	√
C	2012/8/7	220	GF	0.86	WL	0.03	Dif	√	√	√	√	√	20	20	√
C	2012/8/15	228	GF	0.87	WS	0.00	Dif	√	√	√	√	√	20	20	√
C	2012/8/22	235	GF	0.93	W	0.00	Dif	√	√	√	-	√	14	8	√
C	2012/8/28	241	GF	0.86	W	0.00	Dif	√	√	√	No VC	√	8	11	√
C	2012/9/5	249	MA	0.88	WS	0.00	Dif	√	√	√	No VC	√	17	17	√
C	2012/9/11	255	MA	0.88	W	0.00	Dif	√	√	√	√	√	20	20	√
C	2012/9/16	260	MA	0.92	W	0.00	Dif	√	√	√	-	√	20	20	√
D	2012/6/12	164	TL	0.30	WL	-	Dif	√	-	-	√	√	9	-	√
D	2012/6/22	174	TL	0.35	WL	0.08	Dif	√	-	-	√	√	20	-	√
D	2012/6/29	181	TL	0.44	WL	0.11	Dif	√	-	-	√	√	20	-	√

D	2012/7/5	187	FL	0.58	WL	0.06	Dif	√	-	-	√	√	20	-	√
D	2012/7/13	195	FL	0.62	WL	0.10	Dif	√	-	-	√	√	8	9	√
D	2012/7/20	202	FL	0.75	WL	0.06	Dif	√	√	-	√	√	8	8	√
D	2012/7/30	212	FL	0.77	WL	0.11	Dif	√	√	-	-	√	13	20	√
D	2012/8/3	216	GF	0.93	WL	0.09	Dif	√	√	-	√	√	20	8	√
D	2012/8/9	222	GF	0.95	WL	0.05	Dif	√	√	√	√	√	9	15	√
D	2012/8/20	233	GF	0.87	WL	0.02	Dir	√	-	√	√	√	8	17	-
D	2012/8/25	238	GF	0.88	WS	0.00	Dif	√	√	√	√	√	8	20	√
D	2012/9/3	247	MA	0.88	W	0.00	Dif	√	√	√	HM VC	√	20	20	√
D	2012/9/10	254	MA	0.93	W	0.00	Dif	√	√	√	No VC	√	20	20	√
D	2012/9/14	258	MA	1.00	W	0.00	Dif	√	√	√	√	√	14	20	√
															√
E	2012/6/14	166	TL	0.28	WL	0.08	Dif	√	-	-	√	√	20	-	√
E	2012/6/19	171	TL	0.42	WL	0.09	Dif	√	-	-	√	√	20	-	√
E	2012/6/26	178	TL	0.47	WL	0.10	Dif	√	-	-	√	√	20	-	√
E	2012/7/3	185	FL	0.66	WL	0.05	Dif	√	-	-	√	√	20	-	√
E	2012/7/10	192	FL	0.73	WL	0.09	Dif	√	√	-	√	-	8	20	√
E	2012/7/17	199	FL	0.74	WL	0.12	Dif	√	√	-	√	√	9	8	√
E	2012/7/23	205	FL	0.88	WL	0.08	Dif	√	√	-	√	√	20	20	√
E	2012/8/4	217	GF	0.90	WL	0.09	Block	√	√	√	√	√	-	15	√
E	2012/8/8	221	GF	0.89	WL	0.04	Block	√	√	√	√	√	20	20	√
E	2012/8/14	227	GF	0.93	W	0.00	Dif	√	√	√	√	√	20	10	√
E	2012/8/20	233	GF	0.94	W	0.00	Dir	√	-	√	-	√	13	12	-
E	2012/8/26	239	GF	0.93	W	0.00	Dif	√	√	√	√	√	20	20	√
E	2012/9/8	252	MA	0.91	W	0.00	Dif	√	√	√	No VC	√	20	20	√
E	2012/9/14	258	MA	0.92	W	0.00	Dif	√	√	√	√	√	20	20	√

6. Data access and citation

6.1 Data access

All final results over each plot are provided, including PAI, PAI_{eff}, gap fraction, CI, ALA and fCover. They are compiled in ASCII format. Please contact the PI below for the field measured and the processed data.

Prof. Hongliang Fang
LREIS, Institute of Geographic Sciences and Natural Resources Research
Chinese Academy of Sciences (CAS)
11A Datun Road, Room 1318
Beijing, 100101, China
Tel: (8610) 64888055
Fax: (8610) 64889630
Email: fanghl@lreis.ac.cn

6.2 Citation

Fang, H., Li, W., Wei, S., & Jiang, C. (2014). Seasonal variation of Leaf Area Index over paddy rice fields in NE China: Intercomparison of destructive sampling, LAI-2200, digital hemispherical photography (DHP), and AccuPAR methods. Agricultural and Forest Meteorology, submitted.

References

Baret, F., Solan, B.d., Lopez-Lozano, R., Ma, K. and Weiss, M., 2010. GAI estimates of row crops from downward looking digital photos taken perpendicular to rows at 57.5◦ zenith angle: Theoretical considerations based on 3D architecture models and application to wheat crops. Agricultural and Forest Meteorology, 150: 1393-1401.

Demarez, V., Duthoit, S., Baret, F., Weiss, M. and Dedieu, G., 2008. Estimation of leaf area and clumping indexes of crops with hemispherical photographs. Agricultural and Forest Meteorology, 148: 644-655.

Fang, H., Li, W., Wei, S. and Jiang, C., 2014. Seasonal variation of Leaf Area Index over paddy rice fields in NE China: Intercomparison of destructive sampling, LAI-2200, digital hemispherical photography (DHP), and AccuPAR methods. Agricultural and Forest Meteorology, submitted.

Garrigues, S. et al., 2008. Validation and intercomparison of global Leaf Area Index products derived from remote sensing data. Journal of Geophysical Research: Biogeosciences, 113.

Lang, A.R.G., McMurtrie, R.E. and Benson, M.L., 1991. Validity of surface area indices of Pinus radiata estimated from transmittance of the sun's beam. Agricultural and Forest Meteorology, 57(1–3): 157-170.

Lang, A.R.G. and Xiang, Y., 1986. Estimation of leaf area index from transmission of direct sunlight in discontinuous canopies. Agricultural and Forest Meteorology, 37: 229-243.

Miller, J.B., 1967. A formula for average foliage density. Australian Journal of Botany, 15: 141-144.

Nilson, T., 1971. A theoretical analysis of the frequency of gaps in plant stands. Agricultural Meteorology, 8: 25-38.

Norman, J.M. and Welles, J.M., 1983. Radiative transfer in an array of canopies. Agronomy Journal, 75: 481-488.

Ryu, Y. et al., 2010. On the correct estimation of effective leaf area index: Does it reveal information on clumping effects? Agricultural and Forest Meteorology, 150: 463-472.

Song, C., Xu, X., Tian, H. and Wang, Y., 2009. Ecosystem–atmosphere exchange of CH_4 and N_2O and ecosystem respiration in wetlands in the Sanjiang Plain, Northeastern China. Global Change Biology, 15(3): 692-705.

Stenberg, P., 2006. A note on the G-function for needle leaf canopies. Agricultural and Forest Meteorology, 136: 76-79.

Weiss, M. and Baret, F., 2010. CAN-EYE V6.1 user manual.

Weiss, M., Baret, F., Smith, G.J., Jonckheere, I. and Coppin, P., 2004. Review of methods for in situ leaf area index (LAI) determination Part II. Estimation of LAI, errors and sampling. Agricultural and Forest Meteorology, 121: 37-53.

Yang, W., Hao, F., Cheng, H., Lin, C. and Ouyang, W., 2013. Phosphorus fractions and availability in an Albic Bleached Meadow soil. Agronomy Journal, 105(5): 1451-1457.